Research Article Vol. 31, No. 17 / 14 Aug 2023 / Optics Express 28145
Optics EXPRESS

Accurate measurement and adjustment method for interference fringe direction in a scanning beam interference lithography system

YUBO LI,[1,2] SHAN JIANG,[1,4] XINGSHUO CHEN,[1,2] ZHAOWU LIU,[1] WEI WANG,[1] YING SONG,[3] AND BAYANHESHIG[1,*]

[1]*Changchun Institute of Optics, Fine Mechanics and Physics, Chinese Academy of Sciences, Changchun 130033, China*
[2]*University of Chinese Academy of Sciences, Beijing 100049, China*
[3]*College of Instrumentation and Electrical Engineering, Jilin University, Changchun 130012, China*
[4]*jiangshan0122@126.com*
[*]*bayin888@sina.com*

Abstract: To improve the exposure contrast of the scanning beam interference lithography (SBIL) system, a mathematical model of scanning exposure that includes the direction error of the measurement mirror is established. The effect of the angle between the interference fringe direction and the X-axis measurement mirror direction on the exposure contrast is analyzed. An accurate method for interference fringe direction measurement based on the heterodyne interferometry measurement method of the metrology grating and phase shift interferometry is proposed. This method combines the diffraction characteristics of the metrology grating and the phase shift algorithm to calculate the angle between the interference fringe direction and the measurement mirror direction accurately and adjust it. Experiments show that this angle reaches 0.6777 μrad, which meets high-precision grating fabrication requirements. Exposure comparison experiments performed at various angles show that a smaller angle between the interference fringe direction and the measurement mirror direction leads to better grating groove production by scanning exposure, which is consistent with the theoretical analysis. The accuracy of the theoretical analysis and the feasibility of the interference fringe direction adjustment method are verified, laying a foundation for high-quality grating fabrication by the SBIL system.

1. Introduction

Scanning beam interference lithography [1–9] (SBIL) system are used in the fabrication of holographic gratings [10,11]. SBIL is based on the principle that two small-diameter Gaussian beams interfere to form interference fringes. By measuring the platform displacement along the X direction feedback on the phase locking system [12], the phase of the interference fringe changes can be controlled to follow the platform in real time. The interference fringes are then exposed on the photoresist on the grating substrate surface by high-precision two-dimensional platform stepping-and-scanning to form high quality gratings with nanometer-scale accuracy.

During the scanning exposure process, the Y-axis is defined as the scanning direction and the stepping direction is the X-axis. The directions of the interference fringes, the X-axis measurement mirror, and the scanning direction are ideally oriented to be parallel to each other; this ensures the accuracy of the phase stitching and the exposure contrast on the grating substrate during fabrication. However, there is a specific angle between the actual X-axis measurement mirror and the scanning direction that causes the displacement measurement error to be fed back to the dynamic phase locking system [6], which then affects the phase locking accuracy. There is also a specific angle between the direction of the interference fringes and the scanning direction that will reduce the scanning exposure contrast. Therefore, during SBIL system processing for

#485488 https://doi.org/10.1364/OE.485488
Journal © 2023 Received 17 Jan 2023; revised 8 Mar 2023; accepted 25 Apr 2023; published 9 Aug 2023

Optics EXPRESS

holographic grating fabrication, it is essential to know how to measure and adjust the angles of the interference fringes, the X-axis measurement mirror, and the scanning directions relative to each other. To measure and adjust the angle between the interference fringe direction and the scanning direction, Jiang [7] proposed the method of interference fringes based on a metrology grating in 2015. The method used the grating phase shift theorem to adjust the angle between the metrology grating groove direction and the scanning direction. Using the beam alignment system [13], the reflection beam was made to coincide with the diffraction beam using the metrology grating, the angle between the metrology grating groove direction and the scanning direction was adjusted, and an angle range between the direction of the interference fringes and the scanning direction of less than 19 μrad was realized. However, no accurately measured value of the angle was given. In 2019, Li [14] proposed a doubled-period grating (DPG) method to measure the scan angle error in SBIL in combination with phase shifting interferometry (PSI). The method calculates the phase distribution information at both the starting point and the end point in the scanning direction and adjusts the angle between the direction of the metrology grating grooves and the scanning direction. The scan angle error was measured with precision of less than 12.65 μrad. However, this method used the metrology grating minor movement method to obtain the phase shift images, which requires high platform accuracy and stability. The two methods above only consider the angle between the direction of the interference fringes and the scanning direction, and the effect of the phase locking shift caused by the X-axis measurement mirror angle is not considered.

To improve the exposure contrast further, an angle measurement and adjustment method is proposed in this paper based on the interference fringes direction and the X-axis measurement mirror direction being parallel to each other. The principle is as follows. When the platform moves along the scanning direction, because of their relative angles, the X-axis measurement mirror is at an angle that causes a displacement change in the X direction. Simultaneously, the metrology grating also has a change in its phase shift in the scanning direction. The diffraction characteristics of the gratings are combined with PSI to measure and adjust the direction of the interference fringes, calculate the angle between the directions of the interference fringes and the metrology grating grooves, and determine the angle between the directions of the interference fringes and the X-axis measurement mirror. By adjusting the directions of the metrology grating grooves and the two beams, accurate measurement and adjustment of the interference fringes can be obtained that reaches the μrad level.

2. Effect of the interference fringes on SBIL

In the SBIL system, the interferometer-X-axis measurement system measures the platform displacement accurately; this displacement is then fed back to the phase locking system to achieve phase shift in the interference fringes that follow the platform displacement changes in real time, thus enabling exposure to be achieved by stitching the phase fringes and allowing gratings to be produced. Figure 1 shows the exposure scheme of the SBIL system. During the exposure process, system installation errors are unavoidable, as illustrated in Fig. 2. The angle between the direction of the interference fringes and the scanning direction will “broaden” the photosensitive area that remains on the photoresist after exposure, which results in a reduction in the exposure contrast, as shown in Fig. 3(b). In addition, the angle between the measurement mirror direction and the scanning direction that causes the measurement error of the X-axis results in a “mismatch” between the interference fringes that are realized after phase locking control and the ideal interference fringes, which are shown in Fig. 3(c).

In the SBIL system, the beams on both sides are controlled to interfere at the beam waist and form interference fringes. The angular relationships between the direction of the interference fringes, the direction of the metrology grating grooves, the scanning direction, and the X-axis measurement mirror direction are shown in Fig. 4. The angle between the measurement mirror

Optics EXPRESS

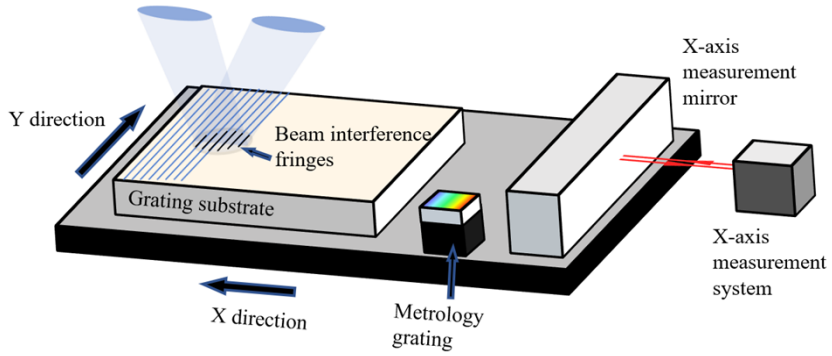

Fig. 1. Schematic diagram of SBIL system during stepping-and-scanning process.

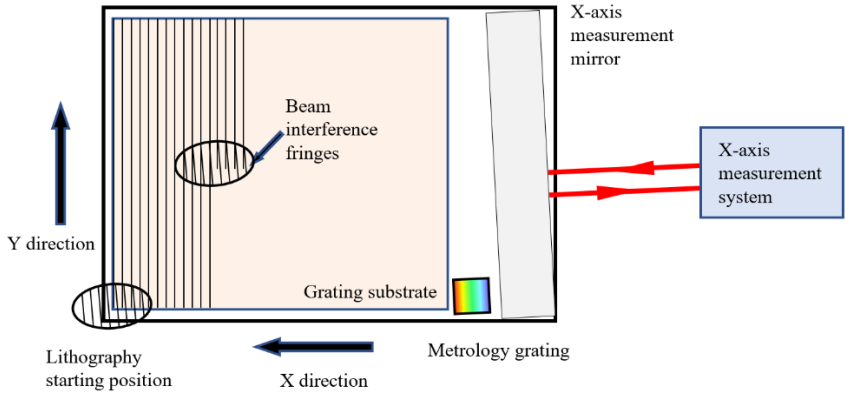

Fig. 2. Schematic diagram of SBIL system during stepping-and-scanning with the direction error of the interference fringes. Vertical view of Fig. 1 with angles.

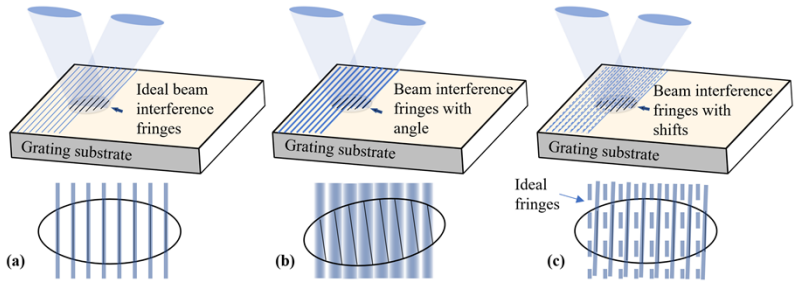

Fig. 3. (a) Ideal interference fringe exposure along the scanning direction. (b) Effects of the angle between the fringe direction and the scanning direction on scanning exposure. (c) Effects of the angle between the measurement mirror direction and the scanning direction on the interference fringe phase shifts.

and the Y direction is α_{m}, the angle between the metrology grating groove direction and the Y direction is α_{g}, the angle between the metrology grating groove direction and the interference fringe direction is α_{f}, and the angle between the beam interference fringe direction and Y direction is α_{θ}. Each beam is a plane wave at the waist and the energy profile is Gaussian. Assume here that the waist radii of the beams on the two sides along the X-axis and Y-axis in the exposure area

Optics EXPRESS

are ω_x and ω_y, their amplitudes are A_L and A_R. The intensity distribution can then be written as:

$$I(x,y,t) = \exp\left[-2\left(\frac{x^2}{\omega_x^2} + \frac{y^2}{\omega_y^2}\right)\right]\left\{A_L^2 + A_R^2 + 2A_L A_R \cos\left[\frac{2\pi}{p_x}(x + \tan\alpha_\theta y) + \varphi(t)\right]\right\} \quad (1)$$

where p_x represents the interference fringe period along the X direction and $\varphi(t)$ is the interference fringe phase shift related to the time that the phase locking system was connected. Define $x_m(t)$ as the X-direction displacement data measured by interferometer at time t of the system, according to the phase locking settings [6], the relationship between $\varphi(t)$ and $x_m(t)$ is:

$$\varphi(t) = \frac{2\pi}{p_x} x_m(t) \quad (2)$$

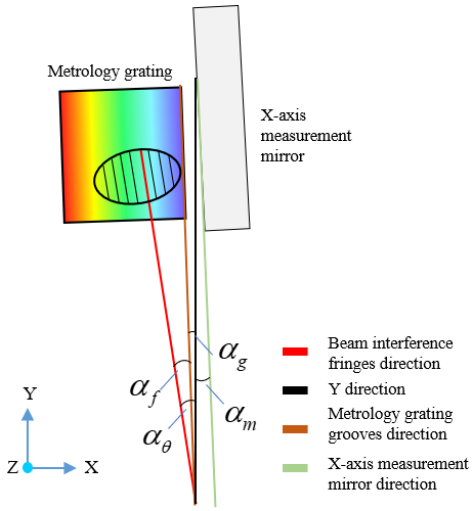

Fig. 4. Relationship diagram of the various angles.

When the angle between the measurement mirror direction and the scanning direction is α_m, the relationship between the X direction displacement data $x_m(t)$ at time t and the Y direction is:

$$x_m(t) = -\tan\alpha_m y(t) \quad (3)$$

By substituting Eqs. (2) and (3) into Eq. (1), we can obtain:

$$I(x,y,t) = \exp\left[-2\left(\frac{x^2}{\omega_x^2} + \frac{y^2}{\omega_y^2}\right)\right]\left\{A_L^2 + A_R^2 + 2A_L A_R \cos\left[\frac{2\pi}{p}x + \frac{2\pi}{p}(\tan\alpha_\theta - \tan\alpha_m)y(t)\right]\right\} \quad (4)$$

During a single scanning exposure process, the stage moves uniformly along the Y direction at a speed of v, where:

$$y(t) = vt \quad (5)$$

A single scanning exposure of any point (x, y) on the substrate can be written as the integral of the interference fringe intensity versus time:

$$D(x,y) = \int_{-\infty}^{\infty} I(x, vt)\,\mathrm{d}t \quad (6)$$

Optics EXPRESS

Substitution of Eqs. (4) and (5) into the equation above then gives:

$$D(x,y) = \frac{\omega_y}{v}\sqrt{\frac{\pi}{2}}\exp\left(-2\frac{x^2}{\omega_x^2}\right)\left\{A_L^2 + A_R^2 + 2A_L A_R \exp\left[-\frac{1}{2}\left(\frac{\pi\omega_y(\tan\alpha_\theta - \tan\alpha_m)}{p_x}\right)^2\right]\cos\left(\frac{2\pi}{p_x}x\right)\right\} \tag{7}$$

The exposure contrast of the platform after the movement along the scanning direction is given by:

$$\gamma = \gamma_0 \exp\left[-\frac{1}{2}\left(\frac{\pi\omega_y}{p_x}\right)^2(\tan\alpha_\theta - \tan\alpha_m)^2\right] \tag{8}$$

where γ_0 is the contrast of the interference fringes in Eq. (1), and

$$\gamma_0 = \frac{2A_L A_R}{A_L^2 + A_R^2} \tag{9}$$

In the ideal case of exposure stitching, the contrast after the stepping and scanning exposure is consistent with that of the single exposure. The Eq. (9) indicates that the contrast of the interference fringes is related to the amplitude ratio of the beams on the two sides. The exposure energy is adjusted to be equal on both sides, which allows $\gamma_0 = 1$ to be obtained. Equation (8) shows that there is a Gaussian function distribution between exposure contrast and the change of $\tan\alpha_\theta - \tan\alpha_m$. The full width at half maximum (FWHM) of the Gaussian function is $p_x/\pi\omega_y$. The FWHM of Gaussian function is proportional to period p_x and inversely proportional to the beam waist radius ω_y in the Y direction of the spot. That is, when p_x is larger or ω_y is smaller, the FWHM is larger, indicating that the change tolerance of contrast to angle $\tan\alpha_\theta - \tan\alpha_m$ is larger. It can also be seen from the Fig. 3 (b) (picture as follows) more intuitively that when the period is larger, the proportion of the period of ‘ fringe blurring ‘ caused by the fringe angle is smaller. When the spot is smaller, the fringe length is shorter, and the influence of the fringe angle is smaller. When the waist radius ω_y of the interference spot in the Y direction and the period of the interference fringes p_x are determined, the exposure contrast γ is related to the square of $\tan\alpha_\theta - \tan\alpha_m$, which is the difference between the tangents to the interference fringes and the

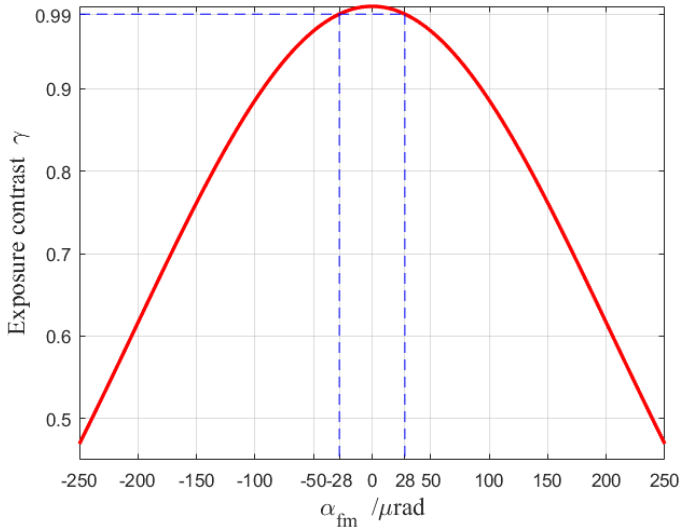

Fig. 5. Relationship between the exposure contrast γ and the angle α_{fm} between the interference fringe direction and the measurement mirror direction.

Optics EXPRESS

measurement mirror. Typically, the values of α_θ and α_m are much less than 1, and the tangent can be approximated to give the angle $\tan\alpha_\theta - \tan\alpha_m \approx \alpha_\theta - \alpha_m = \alpha_{fm}$. This demonstrates that the exposure contrast is related to the angle between the interference fringe direction and the measurement mirror direction. When the interference fringe direction is consistent with the measurement mirror direction, $\alpha_{fm} = 0$, and the exposure contrast $\gamma = 1$. When the system parameter $\omega_y = 0.9$ mm and the interference fringe period $p_x = 574.71$ nm, the change in the exposure contrast with α_{fm} is as shown in Fig. 5. The figure shows that the exposure contrast decreases gradually with increasing α_{fm}, and when α_{fm}<28 μrad, the exposure contrast is greater than 0.99, and the influence of α_{fm} on the exposure contrast is less than 1‰, which meets the exposure requirements.

3. Accurate measurement principle for the interference fringe direction

It can be deduced from the previous section that the angle between the interference fringe direction and the X-axis measurement mirror direction is an important factor that affects the exposure contrast, and it is thus necessary to measure the angle between these two directions accurately. The angle α_{fm} between the interference fringe direction and the measurement mirror direction cannot be measured directly. Therefore, a metrology grating is added to the system as an intermediate element. The angle between the interference fringe direction and the measurement mirror direction is determined based on three angles, as illustrated in Fig. 4.

3.1. Angle between X-axis measurement mirror direction and scanning direction

The X-axis displacement measurement system uses a dual-frequency laser interferometer to perform the measurements. The interferometer system is a four-fold optical subdivision type, and the heterodyne calculation board is a K_1-fold electronic subdivision type. The wavelength of the dual-frequency laser interferometer is λ_m. If the recording exposure starting point $A(x_a, y_a)$ is scanned along the Y direction toward $B(x_a, y_b)$, it can be found that:

$$\Delta x = \frac{\Delta N_1}{4 \times K_1} \times \lambda_m \tag{10}$$

where ΔN_1 is the frequency integral count obtained from the heterodyne calculation board as processed after the stage scans along the Y direction from y_a to y_b, and Δx is the displacement change measured by the interferometer due to the angle α_m between the measurement mirror direction and the scanning direction.

$$\tan\alpha_m = \frac{\Delta N_1}{4 \times K_1} \times \frac{\lambda_m}{y_b - y_a} \tag{11}$$

Therefore, the angle between the measurement mirror direction and the scanning direction α_m can be calculated by recording the displacement change measured by the interferometer when the stage moves in the scanning direction.

3.2. Angle between groove direction and scanning direction of the metrology grating

As shown in Fig. 6, the scanning exposure system uses two Gaussian beams that are exposed symmetrically in the normal direction of the substrate. If a metrology grating with the same groove density as the target exposure grating is placed on the same plane as the grating substrate, the exposure beams on both sides are then diffracted by the metrology grating to meet the Littrow condition; i.e., the incident light coincides with the +1st or −1st orders of the diffracted light. Simultaneously, part of the light that is separated from the optical paths on both sides is returned into detector 1 to act as a phase reference signal after being adjusted using the beam splitter prism. The left beam passes through the −1st order diffracted light of the metrology grating, and

Optics EXPRESS

the reflected light from the right beam is sampled via the beam splitter prism; this sampled light then enters detector 2 as a phase measurement signal. The symbol φ is used to represent the phase information, the subscript L and R are used to represent the left side and right side of the beam, and the suffix -1, 0 and +1 are used to represent the corresponding diffraction order.

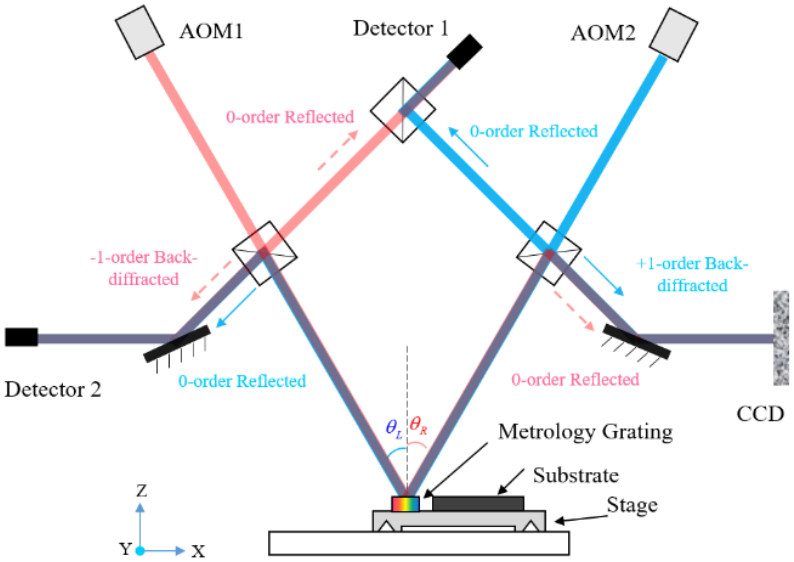

Fig. 6. Schematic diagram of the optical measurement path for interference fringe direction using the metrology grating. CCD: charge-coupled device. AOM1 and AOM2: acousto-optic modulators.

The frequencies of the acousto-optic modulators AOM1 and AOM2 are set such that the exposure beams on the two sides have a specific frequency difference, and detector 1 can then receive the reference phase:

$$\varphi_e = \varphi_{L,0} - \varphi_{R,0} \tag{12}$$

After the beam passes through the metrology grating, detector 2 then receives the measured phase:

$$\varphi_m = \varphi_{L,1} - \varphi_{R,0} \tag{13}$$

The left beam's −1st order diffracted light carries the phase information from the metrology grating:

$$\varphi_m = \varphi_{L,0} + \varphi_g - \varphi_{R,0} \tag{14}$$

The phase of the metrology grating is:

$$\varphi_g = \varphi_m - \varphi_e \tag{15}$$

When the metrology grating is scanned along the Y direction, the following phase shift is received by the detector:

$$\Delta\varphi_g = \varphi_g(y_0) - \varphi_g(y_1) = 2\pi \times \frac{\Delta N_2}{K_2} \tag{16}$$

Here, y_0 and y_1 are the Y direction coordinates of the starting position and the end position, respectively, ΔN_2 is the frequency integral count obtained from the heterodyne calculation board, and K_2 is the corresponding electronic fraction from the board.

When there is an angle α_g between the groove direction of the metrology grating and the scanning direction, and when the metrology grating moves in the Y direction by $\Delta y = y_1 - y_0$,

Optics EXPRESS

then according to the phase shift theorem of the grating, the reflected light on the right side shows no phase shift, and the phase shift of the left side's −1st order beam after passing through the metrology grating is given by:

$$\Delta\varphi_{\mathrm{L}} = \frac{2\pi}{p_{\mathrm{g}}}\Delta y \sin\alpha_{\mathrm{g}} \tag{17}$$

where p_{g} is the metrology grating period, and the phase shift after the dual-beam interference should be consistent with the following phase shifts received by the detector:

$$\Delta\varphi_{\mathrm{L}} = \Delta\varphi_{\mathrm{g}} \tag{18}$$

$$\alpha_{\mathrm{g}} = arc\sin\frac{\Delta N_2}{K_2} \times \frac{p_{\mathrm{g}}}{\Delta y} \tag{19}$$

3.3. Angle between groove direction of the metrology grating and the interference fringe direction

As shown in Fig. 6, the −1st order beam on the left side coincides with the reflected light from the right beam and enters detector 2. The phase shift can be measured accurately using the heterodyne interferometry measurement. If we place a charge-coupled device (CCD) detector symmetrically in the right optical path, the right side's + 1st order diffracted light coincides with the left side's reflected light and enters the CCD surface. Under the condition that the two beams have the same frequency, the interference pattern of these beams can be observed. At the same time, the metrology grating phase information carried from the −1st order diffracted light can be analyzed using the interference pattern received by the CCD, allowing the angle between the direction of the metrology grating and the direction of the interference fringes to be obtained accurately.

The vector direction of the metrology grating is along the $\mathrm{X_g}$ axis, and the groove direction is along the $\mathrm{Y_g}$ axis. If the angles between the left exposure beam and the $\mathrm{X_g}$ and $\mathrm{Y_g}$ axes are β_{Lx} and β_{Ly}, respectively, then the angles between the right exposure beam and the $\mathrm{X_g}$ and $\mathrm{Y_g}$ axes are β_{Rx} and β_{Ry}, respectively, and the four angles satisfy the following conditions:

$$\begin{cases} \beta_{\mathrm{Lx}} = \frac{\pi}{2} - (\theta + \delta_{\mathrm{Lx}}) \\ \beta_{\mathrm{Ly}} = \frac{\pi}{2} - \delta_{\mathrm{Ly}} \\ \beta_{\mathrm{Rx}} = \frac{\pi}{2} - (\theta - \delta_{\mathrm{Rx}}) \\ \beta_{\mathrm{Ry}} = \frac{\pi}{2} - \delta_{\mathrm{Ry}} \end{cases} \quad (\delta_{**} \ll 1) \tag{20}$$

where δ_{**} are the deviation of the incident angle of the left and right exposure beams in the system. The subscript L and R are used to represent the left side and right side of the beam, and the suffix x and y are used to represent the deviation of direction.

According to Eq. (20), the wave vectors $\boldsymbol{k}_{\mathrm{L}}$ and $\boldsymbol{k}_{\mathrm{R}}$ of the two side exposure beams can be written as:

$$\begin{cases} \boldsymbol{k}_{\mathrm{L}} = \frac{2\pi}{\lambda}\left[\sin(\theta + \delta_{\mathrm{Lx}})\boldsymbol{x}_{\mathrm{g}} + \sin\delta_{\mathrm{Ly}}\boldsymbol{y}_{\mathrm{g}} - \sqrt{1 - \sin^2(\theta + \delta_{\mathrm{Lx}}) - \sin^2\delta_{\mathrm{Ly}}}\boldsymbol{z}\right] \\ \boldsymbol{k}_{\mathrm{R}} = \frac{2\pi}{\lambda}\left[-\sin(\theta - \delta_{\mathrm{Rx}})\boldsymbol{x}_{\mathrm{g}} + \sin\delta_{\mathrm{Ry}}\boldsymbol{y}_{\mathrm{g}} - \sqrt{1 - \sin^2(\theta - \delta_{\mathrm{Rx}}) - \sin^2\delta_{\mathrm{Ry}}}\boldsymbol{z}\right] \end{cases} \tag{21}$$

where $\boldsymbol{x}_{\mathrm{g}}$, $\boldsymbol{y}_{\mathrm{g}}$, and $\boldsymbol{z}$ are the directional vectors of the $\mathrm{X_g}$-axis, the $\mathrm{Y_g}$-axis, and the Z-axis in the metrology grating coordinate system, respectively. Because the exposure beam interferes

Optics EXPRESS

at the beam waist, and the wavefront of the laser beam at the beam waist is a plane wave, the interference fringes of the exposure beam at the substrate surface can be written as:

$$I_{z,0} = I_a(x_g, y_g)\cos\left\{\frac{2\pi}{\lambda}[\sin(\theta+\delta_{Lx})+\sin(\theta-\delta_{Rx})]x_g + \frac{2\pi}{\lambda}[\sin\delta_{Ly}-\sin\delta_{Ry}]y_g + \varphi_0\right\} + I_b(x_g, y_g) \tag{22}$$

where $I_a(x_g, y_g)$ and $I_b(x_g, y_g)$ are quantities related to the light intensity distributions of the exposed beams on the two sides, and φ_0 is the phase of the interference fringes at the origin. Equation (22) indicates that the angle α_f between the direction of the interference fringes and the direction (Y_g direction) of the metrology grating grooves satisfies the following:

$$\tan\alpha_f = \frac{\sin\delta_{Ly}-\sin\delta_{Ry}}{\sin(\theta+\delta_{Lx})+\sin(\theta-\delta_{Rx})} \approx \frac{\delta_{Ly}-\delta_{Ry}}{2\sin\theta} \tag{23}$$

According to the properties of beam diffraction, after the beam passes through the metrology grating, the zeroth order reflected light wave vector of the left beam that passes through the metrology grating is given by:

$$\boldsymbol{k}_{L,0} = \frac{2\pi}{\lambda}\left[\sin(\theta+\delta_{Lx})\boldsymbol{x}_g + \sin\delta_{Ly}\boldsymbol{y}_g + \sqrt{1-\sin^2(\theta+\delta_{Lx})-\sin^2\delta_{Ly}}\boldsymbol{z}\right] \tag{24}$$

The wave vector of the +1st order diffracted light of the right beam can be written as:

$$\begin{aligned}\boldsymbol{k}_{R,+1} &= \left(\frac{2\pi}{p_g}-\frac{2\pi}{\lambda}\sin(\theta-\delta_{Rx})\right)\boldsymbol{x}_g + \frac{2\pi}{\lambda}\sin\delta_{Ry}\boldsymbol{y}_g \\ &\quad + \sqrt{\left(\frac{2\pi}{\lambda}\right)^2-\left(\frac{2\pi}{p_g}-\frac{2\pi}{\lambda}\sin(\theta-\delta_{Rx})\right)^2-\left(\frac{2\pi}{\lambda}\right)^2\sin^2\delta_{Ry}}\boldsymbol{z} \\ &= \frac{2\pi}{\lambda}\{[2\sin\theta-\sin(\theta-\delta_{Rx})]\boldsymbol{x}_g + \sin\delta_{Ry}\boldsymbol{y}_g \\ &\quad + \sqrt{1-[2\sin\theta-\sin(\theta-\delta_{Rx})]^2-\sin^2\delta_{Ry}}\boldsymbol{z}\}\end{aligned} \tag{25}$$

The interference pattern I_i of the zeroth order reflected light of the left beam that passes through the metrology grating and the +1st order diffracted light of the right beam that passes through the metrology grating can be written as:

$$\begin{aligned}I_i = I_a(x_g, y_g)\cos\frac{2\pi}{\lambda}\{&[\sin(\theta+\delta_{Lx})+\sin(\theta-\delta_{Rx})-2\sin\theta]x_g + [\sin\delta_{Ly}-\sin\delta_{Ry}]y_g \\ &+\left[\sqrt{1-\sin^2(\theta+\delta_{Lx})-\sin^2\delta_{Ly}}-\sqrt{1-[2\sin\theta-\sin(\theta-\delta_{Rx})]^2-\sin^2\delta_{Ry}}\right]z\} + I_b(x_g, y_g)\end{aligned} \tag{26}$$

Through appropriate adjustment of the optical path, δ_{Lx}, δ_{Ly}, δ_{Rx}, and δ_{Ry} are all much less than 1, and Eq. (26) can then be reduced to:

$$I_i = I_a(x_g, y_g)\cos\frac{2\pi}{\lambda}[(\delta_{Lx}-\delta_{Rx})\cos\theta\cdot x_g + (\delta_{Ly}-\delta_{Ry})\cdot y_g - (\delta_{Lx}-\delta_{Rx})\sin\theta\cdot z] + I_b(x_g, y_g) \tag{27}$$

The CCD surface lies perpendicular to the beam propagation direction and the coordinate system of the CCD plane is established as follows.

$$\begin{cases}\boldsymbol{x}_{ccd} = \boldsymbol{x}_g\cos\theta - \boldsymbol{z}_g\sin\theta \\ \boldsymbol{y}_{ccd} = \boldsymbol{y}_g \\ \boldsymbol{z}_{ccd} = \boldsymbol{x}_g\sin\theta + \boldsymbol{z}_g\cos\theta\end{cases} \tag{28}$$

Optics EXPRESS

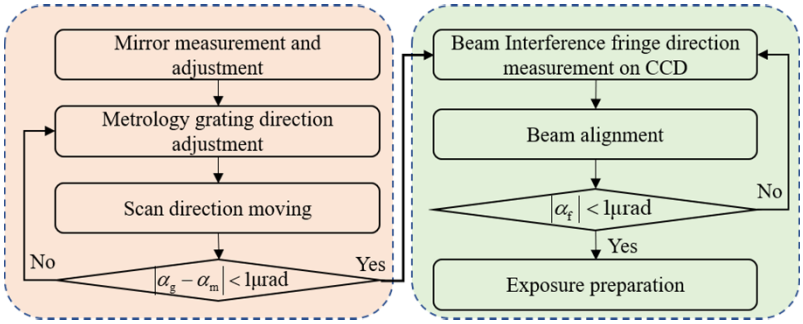

Fig. 7. Flow chart of interference fringe direction adjustment procedure.

Therefore, the exposure beam interference fringes received at the CCD surface can be written as:

$$I_{ccd} = I_a(x_{ccd}, y_{ccd}) \cos \frac{2\pi}{\lambda}[(\delta_{Lx} - \delta_{Rx})x_{ccd} + (\delta_{Ly} - \delta_{Ry})y_{ccd}] + I_b(x_{ccd}, y_{ccd}) \tag{29}$$

Comparison with Eq. (22) shows that by calculating the phase distribution of the interference pattern on the CCD surface, the term $\delta_{Ly} - \delta_{Ry}$ can then be obtained. Substitution of this term into Eq. (23) then allows the angle α_f between the direction of the metrology grating on the substrate surface and the direction of the interference fringes to be measured.

$$\tan \alpha_f = \frac{\delta_{Ly} - \delta_{Ry}}{2 \sin \theta} = \frac{\lambda}{4\pi \sin \theta} \cdot \frac{\partial \phi(x, y)}{\partial y} \tag{30}$$

By adjusting the exposure beam and varying the angles δ_{Ly} and δ_{Ry}, the angle between the scribing direction of the metrology grating and the interference fringe direction can be measured accurately.

4. Experimental results

A straight-line plane holographic grating with a period of 574.71 nm was used as the metrology grating. Using the method described in the previous section, three angles were measured accurately and adjusted. First, the angle α_m between the measurement mirror and the scanning direction was measured and adjusted to be close to the scanning direction. After the stability of the measurement mirror was ensured, the angle α_g between the metrology grating groove direction and the scanning direction was then measured and adjusted to ensure that the difference between the angle α_g and the angle α_m between the measurement mirror and the scanning direction was less than 1 μrad. Then, the angle α_f between the metrology grating groove direction and the interference fringe direction was measured using the interferogram collected by the CCD detector. Finally, an accurate value for the angle between the interference fringe direction and the measurement mirror direction was obtained. The measurement and adjustment process is as shown in the flow chart in Fig. 7.

The stage moves by a distance of 50 mm along the Y direction. The displacement data measured by interferometer and the phase shift data from the metrology grating were collected synchronously. These data were then linearly fitted. The angle between the measurement mirror and the scanning direction was calculated to be α_m = 173.9647 μrad. The angle between the metrology grating groove direction and the scanning direction was α_g = 174.2617 μrad.10 measurements data are shown in Table 1, and linearly fitting data are shown in Fig. 8.

The interferogram collected by the CCD detector after a five-step phase shift [15] is shown in Fig. 9. The phase distribution of the interferogram was obtained using a phase shift algorithm,

Optics EXPRESS

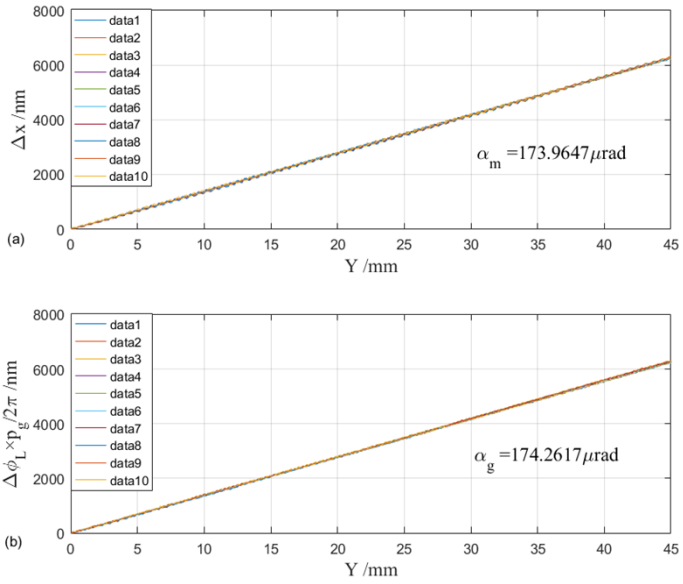

Fig. 8. 10 measurements linearly fitting data: (a) Angle measurements average data for α_{m} between the measurement mirror and the scanning direction. (b) Angle measurements average data for α_{g} between the metrology grating groove direction and the scanning direction.

Table 1. 10 measurements data

	data1	data2	data3	data4	data5
α_m(μrad)	173.9647	173.5190	173.4635	173.4164	173.4600
α_g(μrad)	174.2617	174.5062	174.4402	174.3039	174.5676
	data6	data7	data8	data9	data10
α_m(μrad)	173.4073	173.4431	173.4626	173.4779	172.9611
α_g(μrad)	174.3257	174.2123	174.4220	174.3827	173.8128
Average α_m(μrad)=173.5647			Average α_g(μrad)=174.2617		

with results as shown in Fig. 10. The obtained phase shift phase locking [6] data are shown in Fig. 11, that accuracy is $0.044rad$ $(\lambda/144, 3\sigma)$. By combining these results with Eq. (30), the angle between the direction of the metrology grating grooves and the direction of the interference fringes was then calculated to be $\alpha_{\mathrm{f}} = 0.3807$ μrad.

The angle between the interference fringe direction and the scanning direction is:

$$\alpha_\theta = \alpha_{\mathrm{g}} + \alpha_{\mathrm{f}} = 174.6424\,\mu\mathrm{rad} \tag{31}$$

The angle between the interference fringe direction and the X-axis measurement mirror is:

$$\alpha_{\mathrm{fm}} = \alpha_\theta - \alpha_{\mathrm{m}} = 0.6777\,\mu\mathrm{rad} \tag{32}$$

To verify the accuracy of the measurements and the adjustment of the interference fringe direction, a scanning exposure comparison experiment was performed by varying the angle between the interference fringe direction and the measurement mirror direction. Experimental parameters are summarized in Table 2. To ensure consistency among the exposure and development parameters, exposure was performed on five regions on the same grating substrate. To prevent the beam from introducing other errors during the adjustment process, the direction

Optics EXPRESS

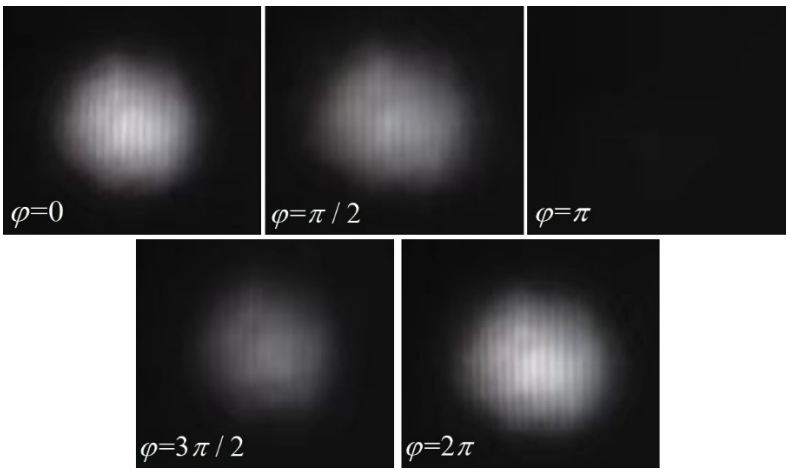

Fig. 9. Interference fringe patterns received by the CCD detector based on the five-step phase shift.

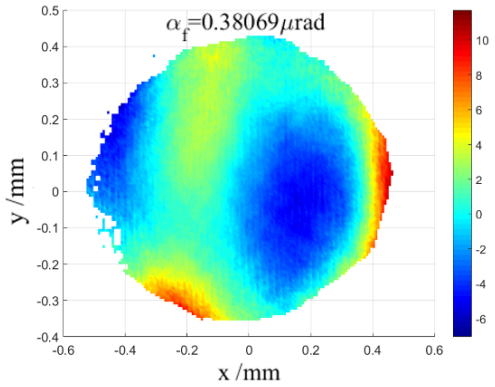

Fig. 10. Angle between the interference fringe direction and the groove direction of the metrology grating.

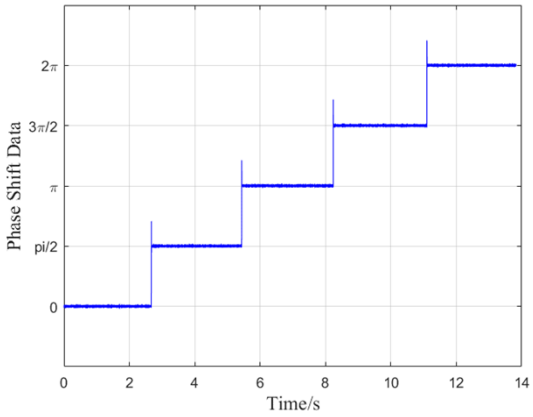

Fig. 11. Phase shift phase locking data.

Optics EXPRESS

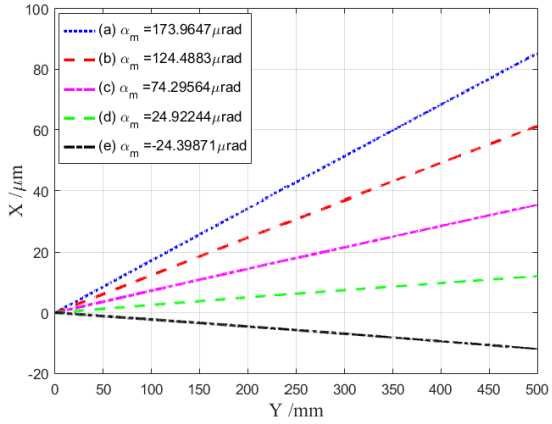

Fig. 12. Displacement changes for the measurement mirror for the same scanning distance at different angles.

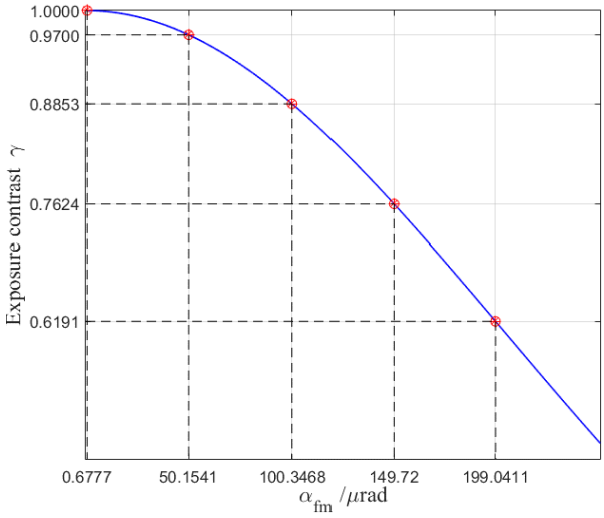

Fig. 13. Theoretical exposure contrasts corresponding to different angles used in comparison experiments.

of the interference fringes remained unchanged, and only the angle of the measurement mirror was varied. The angle measurement data from the measurement mirror are shown in Fig. 12. Angle parameters for all five exposure areas are shown. Based on the previous analysis, the theoretical contrasts γ for the corresponding angle α_{fm} are shown in Fig. 13. As shown in the figure, when the angle between the interference fringe direction and the measurement mirror direction increases, the contrast then gradually decreases. When the angle is 199.0411 μrad, the exposure contrast is reduced to 0.6191, which does not meet the exposure requirements.

Using the parameters presented in Table 3, the exposure was divided into different regions. Each region was then scanned 26 times with a step interval of 0.5 mm, that is, each region was 13 mm and 2 mm apart from the next region. The developed grating is shown in Fig. 14, and the groove shapes in the different exposure regions were measured by atomic force microscopy (AFM), with results as shown in Fig. 15.

Optics EXPRESS

Table 2. Experimental parameters

Photoresist	Shipley 1805
Laser wavelength	413.1nm
Laser power of one beam	0.9mw
Period	574.71nm
Stepping distance	0.5mm
Scanning velocity	50 mm/s
Scanning distance	85mm

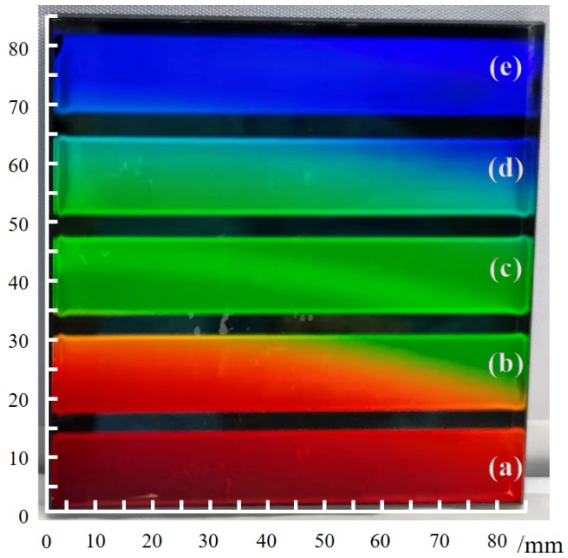

Fig. 14. Comparison of exposure experiment grating mask photographs.

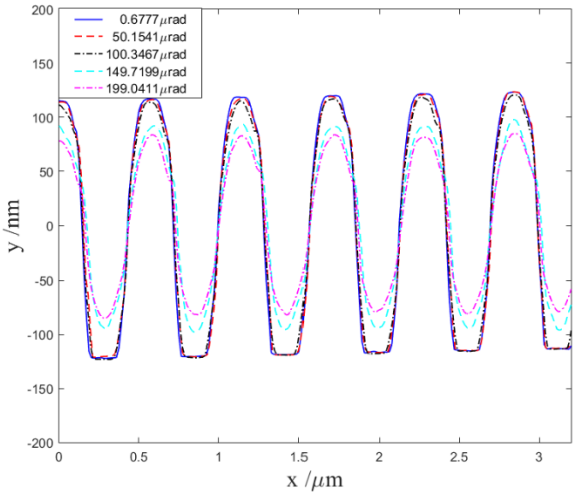

Fig. 15. Mask groove measurements acquired by AFM for comparison experiments.

Optics EXPRESS

Table 3. Angle parameters of the different exposure areas (unit: μrad)

	(a)	(b)	(c)	(d)	(e)
α_{θ}	174.6424	174.6424	174.6424	174.6424	174.6424
α_{m}	173.9647	124.4883	74.29564	24.92244	-24.39871
α_{fm}	0.6777	50.1541	100.34676	149.71996	199.04111

Figure 15 shows that when the angle between the interference fringe direction and the measurement mirror direction is 0.6777 μrad, the grooves of the grating mask are good. When the angle between the direction of the interference fringes and the measurement mirror direction increases, the top of the grating mask groove gradually becomes rounded, and the curvature of the bottom of the groove also increases gradually because of the gradual reduction in the exposure contrast. When the exposure contrast is too low, part of the photoresist is not dissolved completely, the groove shape becomes sinusoidal, and the groove shape quality is seriously reduced. The influence of the angle between the two directions on the exposure contrast is thus verified. Due to the process tolerance of the photoresist characteristics and development process for the exposure contrast, the groove contrast of (a)-(c) in Fig. 15 is not obvious. However, the accurate measurement and adjustment for interference fringe direction provide the greater tolerance for other errors in the system, and lay a foundation for future research on active control of wavefront.

In this experiment, the angle between the interference fringe direction and the measurement mirror direction was adjusted to 0.6777 μrad. This shows that the method for measurement of the interference fringe direction that combines the heterodyne interferometry measurement of the metrology grating with the phase shift calculation can provide significant improvements in the measurement and adjustment accuracy of the interference fringe direction and can also increase the exposure contrast. This is highly significant for scanning of the interference field to enable fabrication of a high-quality holographic grating mask.

5. Conclusion

To improve the exposure contrast of the SBIL system, a mathematical model of scanning exposure that includes the directional error of the measurement mirror has been established. The influence of the angle between the direction of the interference fringes and the X-axis measurement mirror direction on the exposure contrast was then analyzed. An interference fringe direction measurement method that combined the heterodyne interferometry measurement for the metrology grating with PSI was proposed. When the measurement mirror direction was determined, the heterodyne interferometry measurement was then used to measure the angle between the direction of the metrology grating grooves and the scanning direction accurately and then adjust it. The interference pattern of the interference fringes that passed through the metrology grating was collected by a CCD detector; the phase shift algorithm was then used to calculate the phase distribution to determine the angle between the direction of the interference fringes and the metrology grating groove direction and thus obtain an accurate value for the angle between the interference fringe direction and the direction of the metrology grating grooves. The angle could be adjusted to less than 1 μrad by adjusting the exposure beam. Exposure contrast experiments at different angles between the interference fringes and the measurement mirror were also performed. The experiments showed that when using the same process parameters, the grating groove shape worsened as the angle increased, which was consistent with the theoretical analysis. The adjustment accuracy of the angle between the interference fringes and the measurement mirror and its influence on the scanning exposure contrast were verified. In the experiments, after the direction of the interference fringes was adjusted, the angle between the interference fringes and the measurement mirror could be adjusted

Optics EXPRESS

to 0.6777 μrad, which greatly improved the adjustment accuracy of the interference fringes, reduced their influence on the contrast of the scanning exposure, and met the scanning exposure requirements, thus laying a foundation for the production of high-quality gratings by the SBIL system.

Funding. National Key Research and Development Program of China (2022YFB3606100); National Natural Science Foundation of China (61227901, 61905243); The Special Foundation of Science and Technology High-tech Industrialization Cooperation for Advanced Chinese Academy of Sciences and Jilin Province (2021SYHZ0026).

Acknowledgments. This work is supported by National Key Research and Development Program of China (2022YFB3606100); Natural Science Foundation of China (61227901, 61905243); The Special Foundation of Science and Technology High-tech Industrialization Cooperation for Advanced Chinese Academy of Sciences and Jilin Province (2021SYHZ0026).

Disclosures. The authors declare no conflicts of interest.

Data availability. Data underlying the results presented in this paper are not publicly available at this time but may be obtained from the authors upon reasonable request

References

1. P. T. Konkola, "Design and analysis of a scanning beam interference lithography system for patterning gratings with nanometer-level distortions," Ph.D. thesis (Massachusetts Institute of Technology, 2003).
2. C. G. Chen, "Beam alignment and image metrology for scanning beam interference lithography fabricating gratings with nano-meter phase accuracy," Ph.D. thesis (Massachusetts Institute of Technology, 2003).
3. C. G. Chen, P. T. Konkola, R. K. Heilmann, G. S. Pati, and M. L. Schattenburg, "Image metrology and system controls for scanning beam interference lithography," J. Vac. Sci. Technol., B: Microelectron. Process. Phenom. **19**(6), 2335–2341 (2001).
4. J. Montoya, "Toward nano-accuracy in scanning beam interference lithography," Ph.D. thesis (Massachusetts Institute of Technology, 2006).
5. R. K. Heilmann, P. T. Konkola, C. G. Chen, G. S. Pati, and M. L. Schattenburg, "Digital heterodyne interference fringe control system," J. Vac. Sci. Technol., B: Microelectron. Process. Phenom. **19**(6), 2342–2346 (2001).
6. Y. Song, "Research on the interference fringe static and dynamic phase-locking technology in the lithography system of the holographic grating," Ph.D. thesis (Chinese Academy of Sciences, 2014).
7. S. Jiang, "Study on measurement and adjustment of interference fringes for scanning beam interference lithography system," Ph.D. thesis (Chinese Academy of Sciences, 2015).
8. W. Wang, "Study on Beam Quality Control of the Scanning Beam Interference Lithography System," Ph.D. thesis (Chinese Academy of Sciences, 2017).
9. Z. Liu, "Study on wavefront control of grating diffraction on Scanning Beam Interference Lithography System," Ph.D. thesis (Chinese Academy of Sciences, 2017).
10. Z. Qiu, M. Wang, P. U. Yunti, and M. A. Ping, "Investigation progress of laser damage properties on multilayer dielectric film pulse compression grating," J. Mater. Sci. Eng. **35**(2), 329–338 (2017).
11. T. Dietrich, S. Piehler, C. Röcker, M. Rumpel, M. A. Ahmed, and T. Graf, "Passive compensation of the misalignment instability caused by air convection in thin-disk lasers," Opt. Lett. **42**(17), 3263–3266 (2017).
12. Y. Song, Y. Liu, S. Jiang, Y. Zhu, L. Zhang, and Z. Liu, "Method for exposure dose monitoring and control in scanning beam interference lithography," Appl. Opt. **60**(10), 2767–2774 (2021).
13. W. Wang, Y. Song, S. Jiang, M. Pan, and Bayanheshig, "Beam drift error and control technology for scanning beam interference lithography," Appl. Opt. **56**(14), 4138–4145 (2017).
14. M. Li, X. Xiang, C. Zhou, and C. Wei, "Scan angle error measurement based on phase-stepping algorithms in scanning beam interference lithography," Appl. Opt. **58**(10), 2641–2649 (2019).
15. P. Hariharan, B. F. Oreb, and T. Eiju, "Digital phase shifting interferometry: a simple error-compensating phase calculation algorithm," Appl. Opt. **26**(13), 2504–2506 (1987).